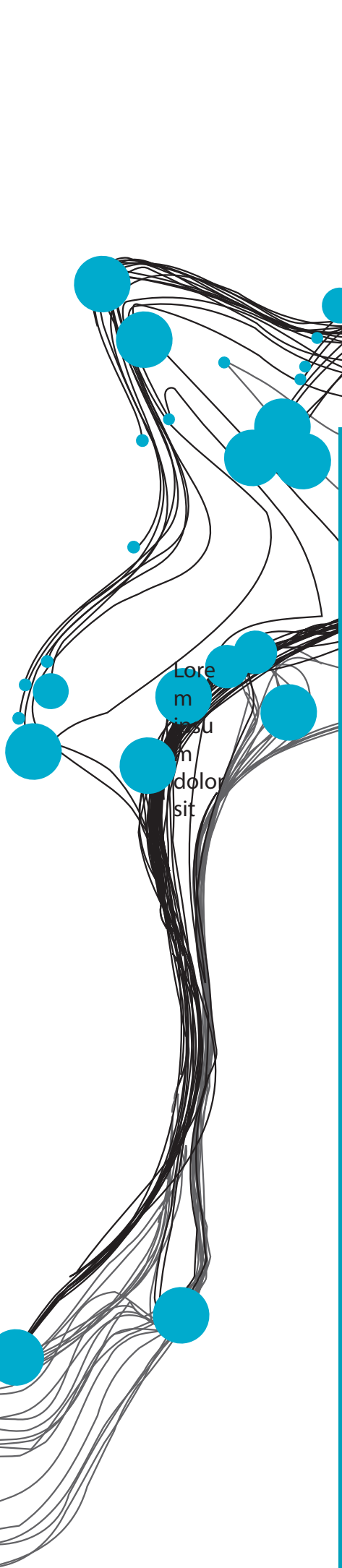

Bachelor Thesis

Theoretical design of the ideal oxygen sensor for intestine-on-a-chip applications

F. Englebert
S1607693

Promotors

Prof.Dr.Ir. L.I. Segerink
E.G.B.M. Bossink MSc
Prof.Dr.Ir. M. Odijk
Dr. J.C.H. Leijten

November 2, 2020

Faculty Science and Technology
Bachelor Biomedical Engineering

BIOS Lab on a Chip group

UNIVERSITY OF TWENTE.

This page is intentionally left blank.

Contents

1 Introduction

December 2019. For the third time in history a Nobel Prize was awarded for a scientific discovery in which oxygen (O2) plays a central role in a physiological process [1]. For centuries it is known that oxygen is an essential parameter for life in mammals, but still, a lot of its functions has remained secret. Although it is well established that most multicellular eukaryotes are aerobic, which means that they need oxygen to obtain their energy efficiently [2], many prokaryotes have developed anaerobic mechanisms to survive.

In the gut the two species live in symbiosis: the aerobic intestinal cells sustain the gut homeostasis together with the anaerobic microbiota. An imbalance between the two is associated with a great variety of pathological disorders, including Crohn's disease, diabetes, colorectal cancer, hepatic steatosis and rheumatoid arthritis [3],[4]. In the past years, investigation of treatment methods (drugs, nutrition, e.g.) for these diseases and the understanding of physiological host-microbiota interactions relied on suboptimal research techniques that did not represent the human's gut effectively. The animal studies that have been done were found unrepresentable for the results in human [5] due to differences in physiology [6]. Additionally, they are costly, require a lot of work and time and they are ethically issued [6], [7]. An alternative to the animal model, is the 2D *in-vitro* model that can cost- and time-effectively predict a cell's behavior against a certain additive. Although this model can provide a solid solution for mono cell culturing studies it is not suitable as a model that represents the systematic physiology of a complete organ in which many cell types interact with each other to sustain its homeostasis [8].

The introduction of intestine-on-a-chip (IoaC) devices promises to overcome these deficiencies in order to create a micro-organ that contains the organ's architectural 3D structure and represents its functionalities to the fullest [9]. The design of the device allows the implementation of multiple cell lines and is based on microfluidic technology in which key parameters, such as concentration, pH, dynamic mechanical stress and cell patterning [7], can be regulated and measured. Despite the advancements aforementioned, there is still a need for development in controlling the culture conditions [10]. Especially for IoaC devices in which controlling the oxygen gradient has appeared to be an essential requirement in order to mimic a gut microenvironment in which the aerobic intestine cells and anaerobic microbiota can live in symbiosis [11].

In order to control the oxygen gradient along the channel of the chip, detection of the oxygen concentration is needed. Currently, various oxygen detection methods can be integrated in the gut-on-a-chip. Conventional methods are optical detection and electrochemical detection [12]. Optical detection uses oxygen-sensitive probes from which the luminescence is related to the oxygen concentration. This method is very sensitive, but lacks in selectivity [13]. Also, the use of probes can be very toxic to living cells [2]. Electrochemical sensors are usually based on redox reactions in which the electron generation is related to the oxygen concentration [12]. Characteristic for electrochemical sensors is its high sensitivity. Depending on the kind of measurement, also a high selectivity can be obtained. A repercussion of the detection method is the local depletion of oxygen around the electrode [14]. Additionally, physical contact of the sensor and the chip's used solution is required [2].

This thesis elaborates on the current status and development of oxygen sensors for IoaC devices. The physiology of the human intestine will be discussed in the second chapter. In the third chapter the architecture of the IoaC device will be explained, consisting of its several components. The fourth chapter provides a more detailed overview of the most frequently used sensor types for oxygen detection in IoaC devices. The fifth chapter sketches the requirements an ideal oxygen sensor for IoaC application must full fill, followed by two innovative proposed solutions in the sixth chapter. Finally, those solutions will be evaluated and future perspectives on promising techniques will be discussed.

2 Physiology

2.1 Physiological architecture and function

The gut, as being a part of the gastrointestinal (GI) tract, consists of several organs that are specialized in digesting food and absorbing nutrients [15]. Among these organs is the small intestine in which nutrients and water is absorbed. This important function can only be provided due to the adapted anatomy of the small intestine (Figure 1) perpendicular organized muscle layers result in peristaltic movement in any dimension, so that the intestine's content is optimally kneaded. The surface of the lumen is maximized by the folded structure of mucosal and submucosal tissue, the circular folds, which has again a folded structure, called the villi [16]. The monocellular mucosal epithelium of the villi mainly consist of tight junction bounded absorptive cells, the enterocytes, that play an important role in the barrier function of the mucosal epithelium [17]. When those cells absorb water and nutrients, it will directly be transported to the blood capillaries and lacteal where it is abducted to the rest of the body. The lumen side of the villi is fully covered with microvilli that form a brush border in which enzymes finish the digestion of carbohydrates and proteins [15]. Microvilli are about 1-1.3 µm [18]. Another important function of the small intestine is protecting the body from pathogens and contributing to the immune system [19]. As described, the architecture and mechanisms of the human intestine tissues are specialized for its functions to optimize both the absorbing of nutrients and the protection against pathogens. Evolution has learned that a symbiosis with microbiota results in a even more efficient way of digesting, producing energy and protecting the body against foreign bodies.

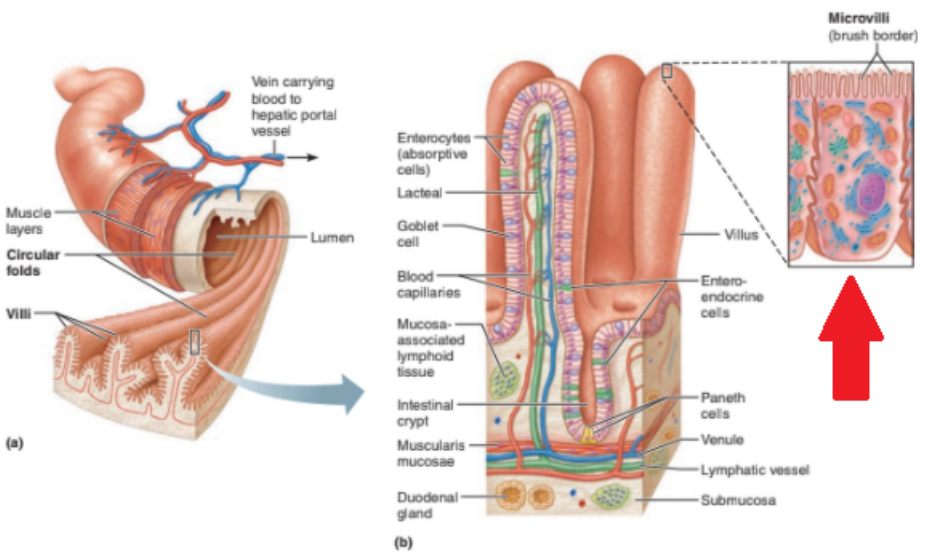

Figure 1: A graphic representation of the small intestine. (a) Perpendicular organized muscle layers contribute to optimal peristalsis. The circular folds and villi maximize the absorption surface within the lumen. (b) The anatomy of a single villus shows the epithelium that separates the in- and external milieu. The epithelium mostly consist of enterocytes which have additionally microvilli on the lumen side. The enlarged enterocyte is indicated by the red arrow. Figure from: [15]

2.2 Microbiota

With trillions of individual microbes, the human intestine is the most densely microbiota packed area of the whole body [20]. Most of the microbes use anaerobic pathways for their metabolism, which differs from the aerobic pathways used in the surrounding intestinal cells. Due to this difference in metabolism, microbiota contribute to the digesting processes and play a major role in the immune system. The symbiosis of the intestinal cells with microbiota have proven to be beneficial for the natural homeostasis of the intestine [19]. Quantitative or qualitative changes in their composition can result in a intestine dysbiosis which is associated with a broad range of

diseases [21]. Additionally, microbiota are also considered to serve as a predictive parameter of response to certain drugs [22]. More investigation on the human intestine-microbiota interaction would therefore not only provide essential information on the derivation of several diseases, but also on drug evaluation. Finally, since every person has a different composition, diversity and function of the microbiota in their intestine, more insight into this topic could potentially lead to personalized treatment methods [19].

2.3 Oxygen gradient

Off all human tissues, the intestinal tissue experiences the steepest oxygen gradient [23]. Since most of the microbiota are anaerobic, a low oxygen concentration is required on the top of the villi. Studies evaluated these strict anaerobic conditions holding a partial pressure of oxygen of only <0.13 kPa [24]. Comparing this to the partial oxygen pressure of 7.1-9.5 kPa at the submucosa [25], a significant increase is observed along the radial axis from lumen to submucosa. In Figure 2 the decrease in partial oxygen pressure is imaged. Figure 2B reflects the change in the slope of the gradient during digestion, showing that this gradient is not a constant value. Despite the different metabolism of the intestinal cells and microbiota, both have evolved several mechanisms to maintain gut homeostasis independently from the local partial pressure of oxygen.

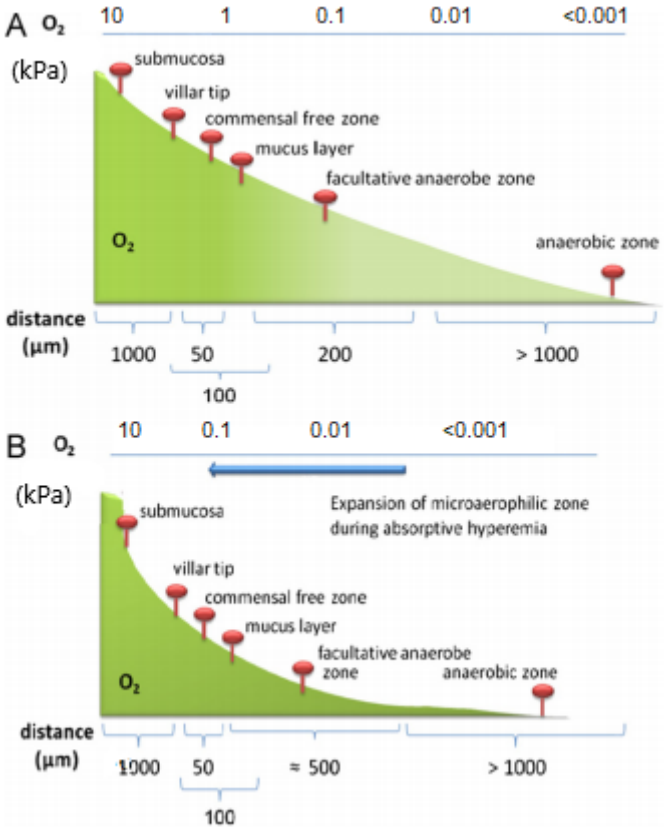

Figure 2: Two graphs reflecting the slope of the oxygen gradient in the intestinal tissue. On the y-axis the partial pressure of oxygen is given and on the x-axis the specific location in the tissue is given. A. Under normal conditions. B. In digesting modus. [23]

3 Intestine-on-a-chip

3.1 Functionalities

Like described earlier, many diseases are associated with the cross-talk between the microbiota and human tissue in the human intestine. Despite of the number of pathological studies that have been performed to map out these interactions, many of the exact mechanisms are still unknown, mainly due to the use of methods that poorly represent the physiological architecture and function of the human intestine. These methods include animal models, two dimensional *in vitro* models and the recently introduced intestine-on-a-chip (IoaC) model. The IoaC model seems a promising method since their major advantages include obtaining three dimensional structures and the ability to control several parameters during the experiments.

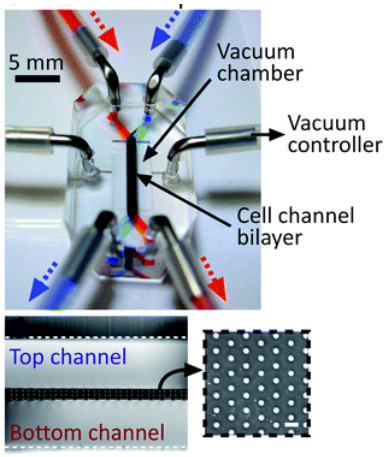

(a) Realistic representation of the IoaC, showing the channels and membrane. Figure from: [26]

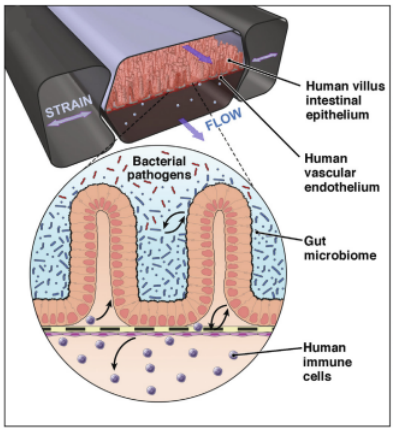

(b) Schematic representation of the Intestine-on-a-Chip model. The membrane (yellow-black striped) separates the intestinal epithelium in the upper compartment from the vascular endothelium in the lower compartment. Both side compartments provide a peristalsis-like strain to mimic the mechanical function of the intestine. Figure from: [27]

Figure 3: Two representations of the Intestine-on-a-chip

IoaC's are microfluidic devices which objective is to mimic the physiological processes of the human intestine. Despite many IoaC devices have been evolved, some characteristics apply to the most of them. The fabrication methods that are used highly rely on the materials that are selected. The materials that are selected, are commonly easy-to-use and optical transparent to allow for optical detection methods. Secondly, most materials are gas permeable to create diffusion possibilities for the metabolic gasses that exist due to the physiological processes of the embedded cells. The general architecture of the devices are two hollow microchannels separated by a membrane (figure 2a). The membrane allows the transport of compounds, e.g. immune cells, from the bottom channel, representing the adjactent vessel, to the upper channel, representing the lumen (figure 2b). Recently, the integration of a physical membrane has been questioned since it does not mimic the *in vivo* like structure optimally [28], impeding progress in the understanding of underlying mechanisms in the barrier function. This has resulted in a shift towards devices without a separating membrane in order to represent the epithelial barrier [29]. To replicate the natural peristaltic movement in the intestine, the design implemented two side compartments that apply mechanical force. The model allows flow rate control and offers the possibility to experiment with a wide range of cells, microbes and compounds that could be found in either the bloodstream or lumen. Other parameters as pH, chemical gradients, mechanical forces can also be controlled and

measured using a IoaC model, making the model applicable for various studies on the intestine and host-microbiota interactions. However, the IoaC model is still being developed and optimized.

Currently, a major drawback of the model is the short culturing time due to the limited diverse oxygen regulation that is a prerequisite for the cocultures of intestinal cells with microbiota to survive [27]. As described earlier in Chapter 2, creating an environment in which oxygen homeostasis can be maintained is a crucial requirement in a microfluidic chip mimicking the human intestine. Providing the right conditions for the aerobe epithelial cells and the complex anaerobe microbiota using a feedback system with an accurate oxygen sensor could serve as a solution.

3.2 Fabrication

IoaC's are produced by micro fabrication involving many different techniques. Standardized protocols can be found online [30]. Methods such as photolithography and soft lithography are generally used to mold the components of the chip [31]. Photolithography uses optical radiation (UV light exposure) to crosslink the photoresist, step c-d in Figure 4. Protecting a part of the photosensitive material with a mask, results in a pattern after removing the non-crosslinked photoresist [32]. Using the obtained master, soft lithography is performed to fabricate a polymeric unit with integrated micro structures and sensors. (step e-f in Figure 4).

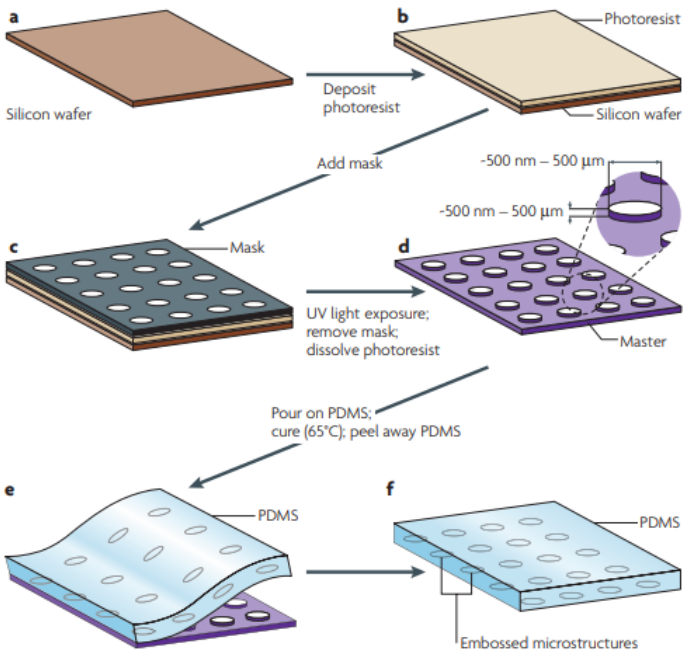

Figure 4: A photoresist is placed upon a silicon wafer. A masked with hollow structures is placed on the photoresist. After exposure to UV light, a master is obtained for soft-lithographic applications. Figure from: [33]

As described above, the common methods to fabricate a chip are based on various steps of lithographic processes, which makes the process time-consuming. Currently, much potential is seen in bioprinting methods. Micro-extrusion, inkjet printing, stereolithography and fused deposition modeling are the bioprinting methods that could be very useful in microfluidic chip development [34].

3.3 Materials

Polydimethylsiloxane (PDMS) is undoubtedly the most frequently used material to create IoaC systems. PDMS is a thermoplastic polymer that is appreciated for its ease of manufacturing and its cell-friendly properties [28]. PDMS offers a bio-inert, non-toxic low adhesive surface, allowing intercellular interaction. Its optical transparency allows the application of optical measurement methods [35]. Despite the fact that PDMS is widely used for IoaC systems, the material has its disadvantages. PDMS is a hydrophobic polymer, attracting lipophilic compounds to its surface. When using optical detection measurements, the luminescent signal can be contaminated by these compounds, resulting in incorrect results. Many studies have been performed on the surface modification of the PDMS in order to reduce the hydrophobicity resulting in less nonspecific adsorption of contaminating compounds. Segregation of smart polymers polyethylene glycol (PEG)-PDMS has proven to reduce the hydrophobicity of the PDMS surface material resulting in less contamination of other compounds [36]. Another disadvantage of PDMS, and specifically for IoaC application, is that it is a gas-permeable material, allowing gas compounds and water vapor to escape from the microchannels. Creating and monitoring the physical hypoxia in the channel can therefore become very challenging. Other materials used in the fabrication of IoaC are glass, polymethyl methacrylate (PMMA) and hydrogels.

3.4 Sensors

Several kind of sensors can be integrated in the chip in order to measure and regulate all kinds of parameters within the microenvironment of the IoaC. Changes in oxygen, temperature, pH, cytokines, nutrients and metabolites can provide valuable information about the mechanisms and interaction of the embedded cells and microbiota. A lot of tissues have an important barrier function to protect the body from pathogens and to transport selective compounds. Especially in drug studies, the barrier function and integrity of an epithilial or endothilial layer can provide cruxial information. Using transepithelial electric resistance (TEER) the barrier integrity and tightness is quantified. It is a widely applied technique for non-invasive assessment of drug toxicity and barrier permeability preditions [37]. Ideally a multi-integrated sensor will be created to limit the total of unknowns, providing optimal monitoring possibilities.

3.5 Cells and microbiota

Generally, at least three types of cultures need to be included in the IoaC device: cells representing the vascular layer, cells representing the intestinal layer and finally, the microbiota for the host-microbiota interaction. Commonly used cells for modeling the vasculature are vascular endothelial cells lines. These include the human umbilical vein endothelial cells (HUVECs) and the human intestinal microvascular endothelial cells (HIMECs) [8]. For the intestinal cell layer the most frequently used cell line is the human epithelial colorectal adenocarcinoma, referred to as Caco-2 [38]. Despite Caco-2 cells are widely embedded in IoaC devices, due to their simplicity, reproducibility, comparable functionalities of intestinal epithelial cells and desired villi-like architecture, the cells are unable to produce a significant mucosal layer [39]. As described earlier in Chapter 2, the mucosal epithelium plays an important barrier function *in vivo*. A limited mucosal layer produced by the Caco-2 cells can therefore not replicate the exact physiological microenvironment of the intestinal epithelium, resulting in insufficient information on the barrier function.

4 Sensor Technologies

Several papers indicate the demand for the monitoring of cell conditions, especially the control of the oxygen gradient [40], [4], [8]. Besides the different methods that are used to detect oxygen, it appears that real-time monitoring has a great interest, because of the direct monitoring and controlling cellular processes. [40], [26], [41]. A lot of the IoaC's nowadays use commercially available sensors, that comprises of either optical or chemical techniques. Because IoaC uses liquid flows through the channel, the oxygen that is detected is dissolved oxygen (DO).

4.1 Optical Sensors

In the past decade, optical sensors has gained a lot of interest. A frequently used method for oxygen detection are the non-invasive sensor spots consisting of luminescent microprobes that produce phosphorescent or fluorescent signals that are calibrated to a certain level of oxygen saturation. The signals are detected by a camera and converted to the oxygen concentration [4]. The technique is characterized by non-invasive. Despite these advantages, optical measurement comes with a couple of disadvantages. Often the technique is time-consuming, because it requires manual sample collection, but more importantly, the results are easily manipulated [40]. Probes can be influenced by surrounding elements and change their luminescence properties by binding with interfering molecules [2]. Also the toxicity of the probe needs to be taken into account to favor the viability of the embedded cells and present microbiota.

4.1.1 Fluorescence

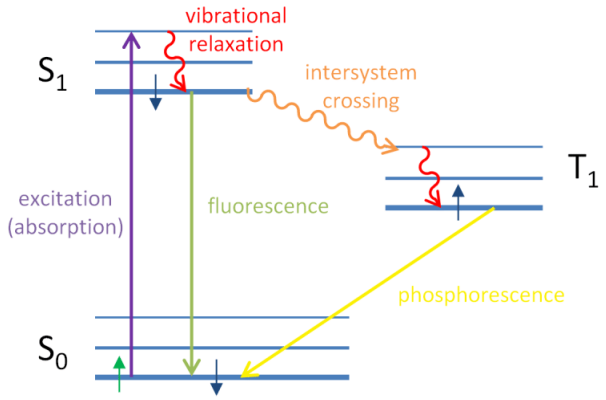

Figure 5: Excitation of an electron from its ground state to higher energy levels. When the compound returns to its ground state, the electron will be emitted as a photon. Short-life emission indicates the green arrow, is fluorescence. Long-life emission, indicates the yellow arrow, is phosphorescence. Figure from: [42]

Luminescence-based probes for oxygen detection can be categorized in fluorescent and phosphorescent probes. The theory behind luminescence relies on the Stokes shift principle in which the absorption of light with a specific wavelength causes emission of light with larger wavelength [14]. The Jablonski diagram in Figure 10 is used to sketch the different energy states of a single atom and to support the understanding of this principle. If light strikes the probe, light of a specific wavelength is absorbed, resulting in an electron that is exited from its ground state S_0 to the higher energy state, S_1. From this state there are two pathways to return back to the stable ground state. When the probe returns directly from S_1 to S_0, a photon of a larger wavelength than the absorbed light will be emitted, since the electron has lost some energy due to vibrational relaxation in the excited state. This process is called short-lived emission and the emitted photon correlates to fluorescence. In the second process intersystem crossing causes the probe firstly to be in an energy state that is more energetically favorable (T_1) than S_1. From here the probe slowly relaxes to the ground state by emitting a photon of an even longer wavelength than in the first

described pathway. This photon correlates to phosphorescence. The time it takes for a compound to return from its excited state to its ground state is called the quenching time. Short-lived emission has a quenching time between 10^{-9} to 10^{-7} seconds, while long-term emission can take up to 10 seconds [42]. As mentioned earlier, IoaC devices focus on real-time measurement, so fluoresce measurements are preferred, reflecting changes more rapidly. Also, due to their longer quenching time, phosphorescent are more like to suffer from contamination by other compounds.

An oxygen sensitive luminophore transfers its excited state energy to neighbouring oxygen instead of emitting this energy as a luminescence photon. Therefore the total luminescence intensity will be decreased. The exact luminescence intensity can be linked to the total occurring transfers, so the total of oxygen molecules the energy is transferred to. The following equation shows how the partial pressure of oxygen is related to the luminescence intensity. The equation is known as the Stern-Volmer equation [43]:

$$\frac{\tau_0}{\tau} = \frac{I_0}{I} = 1 + k_Q \tau_0 pO_2, \tag{1}$$

with pO_2 as the partial pressure of oxygen, k_Q the quenching rate constant, I_0 and τ_0 the luminescence intensity and the excited state lifetime in the absence of oxygen, respectively and I and τ the luminescence intensity and the excited state lifetime at the partial pressure of interest.

In recent studies, the oxygen concentration is often measured using fluorescence emitting sensor spots or optodes. The sensor spots are sprayed on the in- and outlets of the channels in the chip. The HuMiX device, a device that consists 3 chambers, seperating the microbiato from the intestinal tissue, uses integrated optodes to monitor the oxygen concentration in each chamber. In another study from Shin et al. inert platinum dendrimer-encapsulated nanoparticles (Pt-DENs) catalyse the oxidation of Amplex Red, which produces the highly fluorescent resorufin in the presence of molecular oxygen. The fluorescent signal was analyzed with confocal microscopy in the XZ-plane and calibrated to obtain a quantitatively measurement of the concentration of oxygen [44].

4.2 Electrochemical Sensors

Electrochemical sensors used for oxygen detection in bioassays are based on a sub-class of the voltammetry technique, namely amperometric sensors [45]. Amperomeric sensors rely on the redox reactions of electroactive species. During this redox reaction, an electrical current is generated and measured, which can be related to the concentration of the species in the sample. Below the redox reaction is given for acid and neutral solutions, because those are most often used in as electrolyte in the sensor:

$$O_2 + 2H_2O + 4e^- \rightarrow 4OH^- \tag{2}$$

The basis of the amperometric sensor lies within the Clark-type sensor. This type incorporates a noble metal electrodes [46],[47]. Often a platinum electrode as working electrode (cathode),which potential is set around -800mV [48] and a silver/silverchloride reference electrode (anode).

For years the Clark-type sensors have been used as the oxygen sensors due to its reliability [14]. Despite the commercial version of these sensors are still widely used for several applications, it doesn't seem the optimal method for microdevices due to its bulky appearance. Also, as can be seen in figure 6 the electrodes needs to be in physical contact with the solution for detection [2]. The redox reaction that is needed for detection of the oxygen concentration is causing oxygen depletion along the cathode which can cause errors. The generated electrical signals also influence the cultured cells in *in vitro* application, which can result in inaccurate data. Finally, the sensor is sensible for biofouling which can impede oxygen from being reducted at the working electrode and therefore decrease the sensor's sensitivity. Bossink et al. applied surface modification of the sensor to offer a solution to this biofouling. Using the polymer poly(hydroxyethyl methacrylate) (pHEMA) they designed a biocompatible sensor that could be placed in direct contact with the cells [46]. Wu et al. proposed on of the first miniaturized Clark-electrodes for microfluidic devices [49].

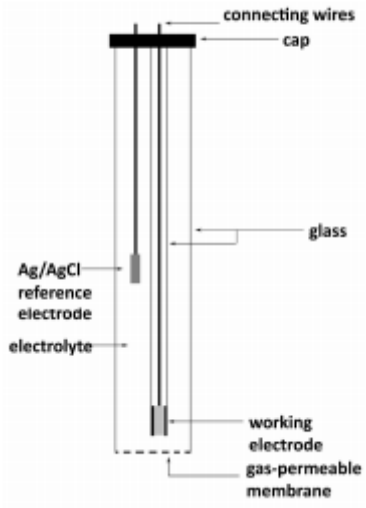

Figure 6: Schematic representation of the Clark electrode. The electrodes need to be in contact with the electrolyte for detection. Figure from: [47]

Inkjet-printing has introduced a new method of the printing of electrical sensors, which miniaturizes the sensor's appearance. It has the desired sensitivity that can be provided by the Clark-type sensor, but is also applicable to microdevices and easily implementable in its production process[26]. Using biocompatible inks, it can be an interesting method for oxygen detection in IoaC's [50]. In Figure 7 shows the production process of inkjet-printed electrochemical sensors. The process

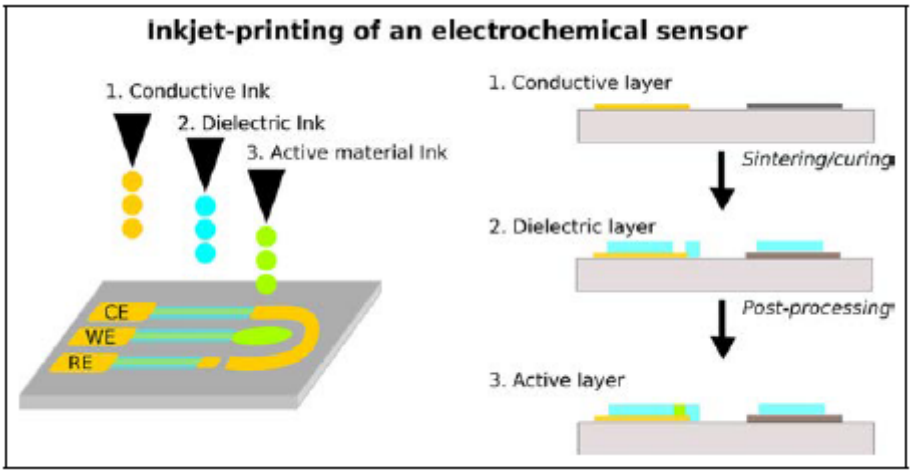

Figure 7: Representation of the inkjet printing process. Figure from: [50]

uses a combination of conductive inks (mostly metals) and a dielectric material that protects the conducted path and forms an area for the active sensing area. Inkjet-printed sensors can be produced very thin (100-500 nm) and can be easily integratable in IoaC devices. Different from the traditional Clark-electrode (Figure 6), the printed sensor consists of three electrodes: a working electrode, reference electrode and a counterelectrode which closes the current circuit. Moya et al. produced an inkjet-printed DO sensor for real-time measurement that only used a small amount of oxygen. However, the method is still depletes oxygen, which is not favorable in cultures that need to maintain an anoxic environment. Recently, a new Clark-type oxygen microsensor was proposed for integration in organ on a chip devices. This sensor doesn't consume analytes and therefore conquers the disadvantage of oxygen depletion along the electrode [51].

4.3 Overview Sensor Technologies

Sensor Technology	Compatible with IoaC	Sensitivity	Biocompatible	Response time
Electrochemical				
Miniaturized Clark-sensor [49]	yes (18 x 26 mm)	-	Yes	6.8 seconds
Zero-consumption Clark-type [51],[52]	Yes	121 nA*cm^2*^{1}	Yes	< 7 seconds
Inkjet-printed DO [50]	Yes, easily integratable	28 nA*L*mg^{-1}	Good	60 s
Optical				
Optode [26],[53]	Yes (5mm diameter)	0.03%	Good	<40 seconds
Fiber Optic [54],[55]	Needle	0.007%	Good	<10 seconds
Pt-DENs + Amplex Red	Yes (integrated in culture medium)	-	Yes	<10 seconds

Table 1: In this table a small overview is given of the technologies that were mentioned in the Chapter. The features will be used to set the requirements of an oxygen sensor for IoaC applications.

5 Requirements oxygen sensor

In order to compose the ideal sensor for intestine-on-a-chip applications the most important requirements can be derived from the knowledge described in Chapters 3 and 4. The architecture of the chip must be taken into account. The purpose of the sensor is to measure the oxygen concentration within the chip to determine and control the oxygen gradient. Like described in Chapter 2 different oxygen concentrations should be obtained for the human epithelial cells comparing to the microbiota. This comprises the measurement of at least two different locations: at the layer of the microbiota and at chip's membrane. In Figure 8 the dimensions of the desired chip are visualized. The following requirements are ranked from most important to less important.

1. **Bio-compatibility**
   If the sensor uses/contains compounds that could be toxic to either the cells or the microbiota, measures should be taken. Cell viability studies should be 95% at least.

2. **Sensor placement in the IoaC**
   Deduced from the intestine's physiology at least two sensors are needed for the oxygen gradient control within the chip. The first sensor should be able to measure the oxygen concentration in the upper channel. The second sensor should be able to measure the oxygen gradient of the bottom channel. However, this placement has proved to limit the control oxygen gradient over the radial axis of the tissue, since intestinal crypts and local accumulation of microbiota can manipulate the data obtained by only one sensor. Ideally, a sensor is needed that can measure the oxygen concentration over the radial axis of the tissue. Multiple sensors can be used over the total length of the channel.

3. **Dimensions**
   As can be seen below, the surface area of the membrane that separates both microchannels is 100 x 1 x 0.02 mm. To measure the concentration over the full length of the membrane, this means that the sensor should be able to measure over the area 100 x 1 mm.

   The height of a villi varies from 0.5-1.6 mm (including the microvilli layer of 1mum). Addition of a microbiota of several layers of bacteria (50 mum), the upper channel's vertical dimension would be 2 mm. The second chip can therefore only measure up to 0.4 mm vertically.

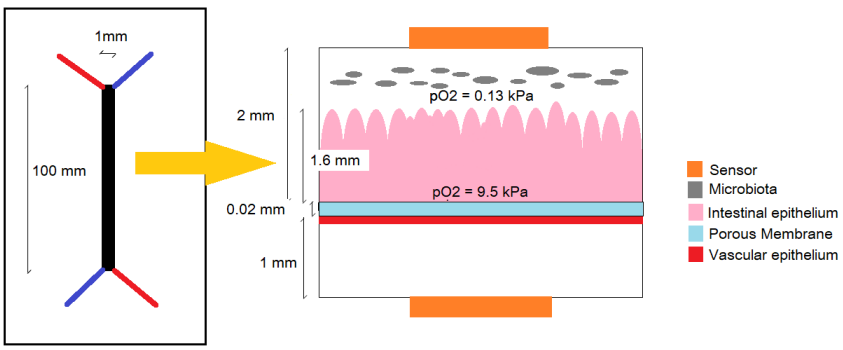

Figure 8: For the design of the ideal oxygen sensor for IoaC applications, the model was sketched representing the desired dimensions. On the left a top view of the chip is given and on the right the vertical intersection of the microchannels is enlarged indicated by the yellow arrow. Also the desired oxygen concentrations are stated at the specific location in the upper channel. The upper and lower channel are separated by the porous membrane in blue. The placement of the sensors is visualized in orange, the size of the sensor can vary.

4. **Response time**
   The sensor must be able to perform real-time measurement in order to create a chip in which the oxygen gradient can be continuously controlled. To limit the amount of data, time-intervals of 10 minutes can be chosen for oxygen concentration measurement. This is in line with earlier performed studies monitoring the oxygen concentration [26]. The response time of the sensor must be 10 seconds.

5. **Endurance of regular deformations**
   The sensor must endure the mechanical stress that mimics the peristaltic movement in the chip. According to the human intestinal model presented by Kim et al. an *in vivo* like mechanical microenvironment can be obtained by applying a cyclic stretching regimen of 10% in mean cell strain with a frequency of 0.15 Hz [3]. The maximum applied pressure for characterizing the parameters was 45 kPa. The pressure applied in order to obtain the 10% cell strain during the study was much lower, around the 18 kPa.

6. **Sensitivity**
   The sensitivity of the sensor is of great importance in this application, since any small change in oxygen concentration can lead to cell death or death of the microbiota. Since the microbiota are living under strict anoxic conditions (<0.13 kPa O_2), small changes need to be detected. Therefore the ideal sensitivity of the sensor needs to be 0.01 kPa O_2.

Nice to have:

1. Concurring current development, the proposed solution also needs to be able calibrate itself[10]. Especially in long-term measurement studies, biofouling, reduction of the electrodes conductivity or a probe's fluorescence intensity can manipulate the data. Recalibration is therefore needed. Time will be saved and data will be more trustworthy when the sensor doesn't need to be calibrated again.

2. The detection methods needs to be easily implementable in the fabrication of the chip.

3. Data for acquisition, visualization and storage.

6 Proposed solutions

6.1 Oxygen sensitive microbeads integrated in hydrogel

With the introduction of 3D printable hydrogels for biomedical scaffold applications ECM constructs for the epithelial intestines layer could be fabricated [56]. As earlier described in Chapter 3, one of the disadvantages of the use of Caco-2 cells is that thy are incapable of creating the intestinal mucosal layer [57]. A scaffold that mimics the architecture of the biological tissue can support the Caco-2 cells in order to form a more stable and *in vivo* like structure. Creff et al. have succeeded in fabricating a 3D hydrogel-based scaffold on which cells are printed. The results show a 3D culture model that mimics the intestinal epithelium that supports the tissue for 3 weeks [58]. Although a scaffold can be fabricated in which intestinal cells can be embedded, there is also the possibility to simultaneously print the cells, the hydrol and the microbeads [59]. Microbeads could possibly serve as an alternative for the optical spots, as the fluorescent particles can be gradually dispersed over the complete membrane area, providing spatial information about the oxygen concentration. This method can also pave a way to the artificial membrane-less IoaC model that is investigated right now.

6.1.1 Oxygen sensing microbeads

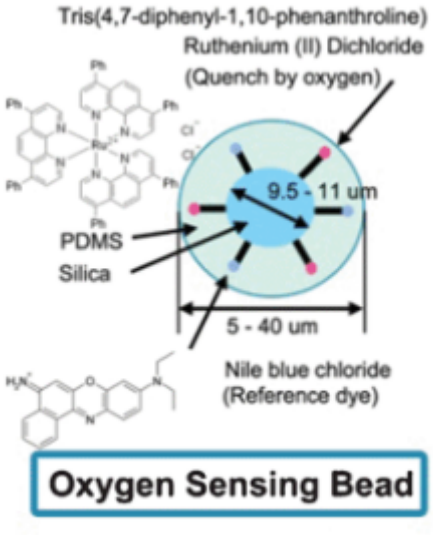

Figure 9: The oxygen sensing microbead fabricated by Wang et al. Containing a silicon core and PDMS shell. The oxygen sensing dye used was Ruthenium(II)Dichloride and the reference dye was Nile blue chloride. Figure from: [60]

.

The microbeads that will be dispersed in to the hydrogel needs to be non-toxic and permeable to oxygen for probe detection. Wang et al. have accomplished to fabricate optical oxygen sensing microbeads for real-time monitoring of the oxygen concentration within cultivated Caco-2 cells [60]. In figure 9 the design of an individual bead is visualized. The bead consists of a silicon core, which causes the particle to be large, resulting in a large surface for oxygen detection by the probes [61]. The fluorophore Ruthenium(II)Dichloride is found to have a high sensitivity for oxygen, with a sufficient biocompatibility [62]. As described in Chapter 4 Ruthenium is one of the most frequently used luminophores in optical oxygen detection methods, which has proved its functionality and biocompatibility. Cytotoxic assays with the reference fluorophore Nile Blue have provided high cell viabilities [63], allowing it to be a sufficient compound for applications within living tissues. Nile Blue is insensitive to oxygen and is therefore not quenched during the measurement. It provides a constant fluorescent signal during the measurement with a different

wavelength (Ex/Em = 636/656 nm) than that of Ruthenium (Ex/Em = 470/610 nm), so their response signals can be easily distinguished. The fluctuating fluorescence caused by Ruthenium is reflected to the reference dye as a measure of change. The shell of the microbead consists of PDMS which is, as already mentioned in Chapter 3 a biocompatible and gas-permeable material, allowing oxygen to diffuse through the shell.

6.1.2 3D printed scaffold

Inkjet-printing needs fluidic ink, which makes it an ineligible method for printing the intestinal scaffold [64]. The combination of microbeads, hydrogel and Caco-2 cells are expected to cause a too high density of the printing material for this method. Kim et al. fabricated an intestinal villus epithelium using the extrusion printing method with a cell-laden collagen bioink [59]. The embedded cells obtained an initial cell-viability of ¿90% and were cultured for 30 days. Extrusion is the most frequently used 3D printing technique and uses thermoplastic materials to print. In order to print these materials, the nozzle contains a heating element that causes the thermoplastic material to semi-melt [65]. This, initially static, scaffold with villi like structures (Figure 10) will be printed along the total length of upper channel on top of the membrane as described in the proposed dynamic model of Chapter 5.

Figure 10: The desired 3D printed scaffold for the IoaC. The scaffold will exist of hydrogel, oxygen sensing microbeads and living Caco-2 cells. The model was earlier fabricated by Kim et al. using a cell-laden collagen bioink. Figure from:[59].

6.1.3 Fabrication

In order to create a hydrogel that has integrated oxygen sensing microbeads, different procedures must be performed. All protocols can be found in Chapter 9, the Appendix. In the first step, the microbeads are fabricated. This fabrication process takes 2 days. After this process the microbeads can be characterized by Dynamic Light Scattering for their seize distribution and by Scanning Electron Microscopy to inspect their physical appearances. Before the microbeads can be integrated within the hydrogel, the beads need to be added to cultured cells for a cytotoxicity assay. After adding the microbeads to the embedded cell culture, it takes 2 days before the cytotoxicity of the beads can be analyzed. When the microbeads show biocompatible results, the microbeads can be integrated in the hydrogel. This process takes 4 days in total. Next,the hydrogel with integrated microbeads can be printed in the upper channel and the standardized production process of the chip (as decribed in Chapter 9) can be finalized.

6.1.4 Detection methods

First of all the sensing beads are calibrated, using a fluorescence intensity assay between the DO concentration range of 0 - 18 kPa. A confocal microscope in the XZ-plane is used for the spatiotemporal detection of the fluorescence. With the Stern-Volmer equition from Chapter 4, the calibration curve can be used to obtain the queching constant:

$$\frac{I_0 - I}{I_0(f_1 - 1) + I} = k_Q p O_2 \tag{3}$$

In which I_0 and I are respectively the intensities of $I_{Ruthenium}$ divided by $I_{NileBlue}$ at 0 kPa and 18 kPa. The linear regression is indicated by f_1 and the quenching constant by k_Q. This step is also important to normalize the eventual difference in distribution of the microbeads within the scaffold.

The penetration depth of confocal microscopy is limited by 100 μm. This means that for the described *in vivo* like dimensions described in Chapter 5, it would be impossible to measure throughout the length of a villi of 1.6 mm. This means that either the architecture has to be minimized or the detection method needs to be chosen differently.

The resolution of bioprinting using extrusion is in the range of 50-500 μm [66], which means that the villi like structure can be minimized. However, the diameter of a single Caco-2 cell is about a 100 μm [67], so the architecture needs to be at least 1 mm in order to create a 3D dimensional villi-like tissue.

Deeper penetration depths can be obtained by using low frequency light, Near Infrared (NIR). The penetration depth of NIR is in the range of 700-900 μm [68], which would make it possible to detect the fluorescence in a miniaturized villi model.

6.2 Using evolutionary evolved oxygen sensors

One of the main drawbacks of the use of probes for optical oxygen detection is the selectivity. In healthy human cells this oxygen detection must be selective. Zooming in on the physiological processes in the human body that are responsible for the maintenance of the oxygen homeostasis, two groups of enzymes seem to play a major role: Prolyl hydroxylases (PHDs) and NADH oxidases [69] [70]. Both groups have different interactions with oxygen as PHDs require molecular oxygen for their activation, while NADH oxidases reduce oxygen reactive species (ROS). For the design of the oxygen sensor is chosen to elaborate on the PHDs, since the interactions of PHDs can be directly linked to molecular oxygen consumption.

6.2.1 Prolyl Hydroxylase

In the human body, there exist three prolyl hydroxylases (PHD1, PHD2 and PHD3). PHDs are known for their role in the hypoxia regulating pathway [71]. In normoxic conditions they target the oxygen-sensitive terminus of the hypoxia-inducible factor (HIF) subunit α to hydroxylate and thereby diffuse the HIF protein. Of all three, PHD2 is the critical oxygen sensor setting the low steady-state levels of HIF-α in normoxia [72]. HIF is a basic helix-loop-helix transcription factor with subunits α, which is oxygen-sensitive, or β, that regulates the oxygen homeostasis in almost all cell types [24]. In figure 11 the HIF pathway is schematically visualized in normoxia and hypoxia environments. In normoxia HIF-α is degraded by the Von Hippel-Lindau (VHL) protein after its hydroxylation due to PHDs. In hypoxia the oxygen concentration is too low for PHDs to hydroxylate the HIF-α, which allows the protein to translocate to the nucleus where it forms a complex with HIF-β and p300 in order to transcript the HIF target genes for hypoxia response.

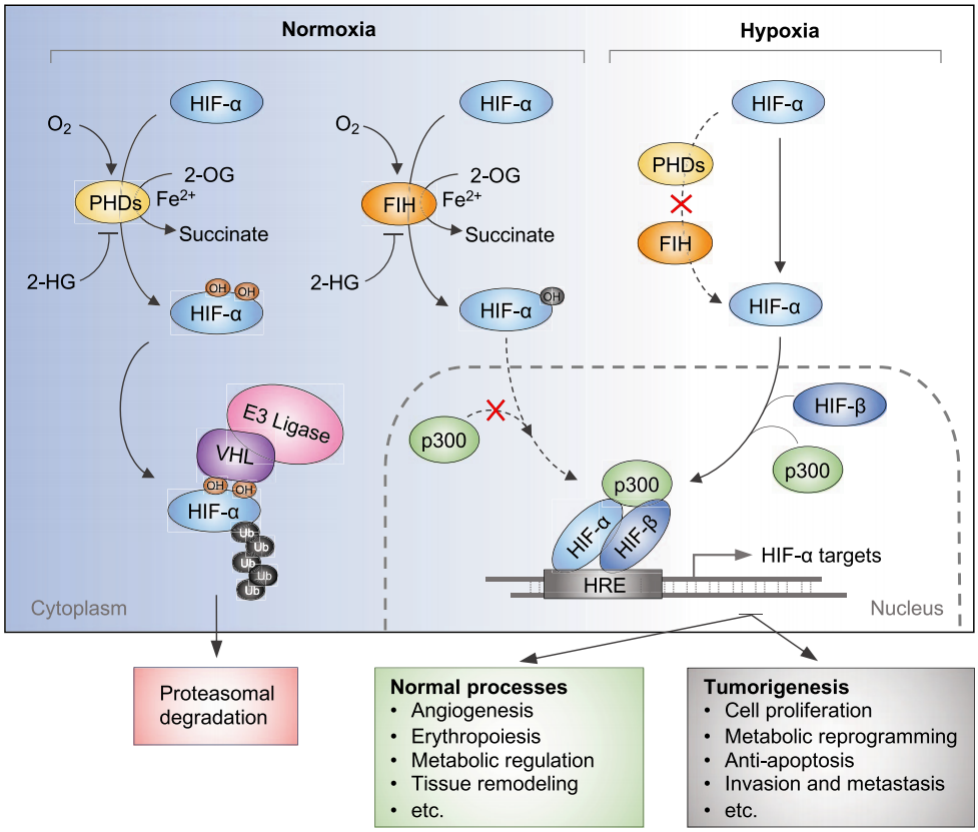

Figure 11: Schematical representation of the HIF pathway. Figure from: [24]

6.2.2 Methods

The suggested method for detecting the real-time oxygen concentration is by using fluorescent labeling of the active enzyme prolyl hydroxylase. In the past years several techniques have been evolved to target and monitor specific proteins in various cellular processes [73]. Ning et al. [74] presented a strategy in which they developed an two-photon fluorescent probe for the oxidative target enzyme CYP3A4. Their strategy showed a high selectivity and specificity and could be used for real-time measurement. Two-photon microscopy has a limited background signal and can reach a penetration depth of 600-800 μm, using NIR. Therefore it is superior to the traditional fluorescence microscopy techniques [75]. Probing PHDs using dealkylation, comparable to the targeting strategy as performed by Ning et al. and implementing them in the fluid flow of the upper and lower channels of the chip, provides a distribution within the chip of the enzyme.

However, it should be noted that this approach will not result in quantitative data on oxygen concentrations, it would only provide information of normoxic cell conditions vs. hypoxic cell conditions.

7 Discussion

Over the past decades, a broad spectrum of organ on a chip devices have been developed. Still, there is a lot ongoing research to different components of the chips, like chip material, embedding cell cultures and sensory systems. It must be noted that the current materials used in the fabrication of the IoaC seem inadequate to mimic the intestine tissue and its functionalities regarding host-microbiota interaction. 3D printing techniques seem promising techniques for exact tissue replication.
von Martel et al. questioned GoaC for being eligible for maintaining anaerobic conditions in the small diameter of the channels [76].

For IoaC devices a major challenge is to include microbiota and sustain and regulate the oxygen gradient over the radial axis of the intestinal tissue. Frequently used detection methods, including optical and electrochemical sensing have been insufficient in their application to regulate oxygen gradient control in the IoaC.

While no experiments have been performed, the *oxygen sensing microbeads integrated in a hydrogel for 3D printing* and the *Prolyl Hydroxylase probes*, can be evaluated using existing papers on comparable applications.

Biocompatibilty
The biocompatibility of the microbeads is tested before integration in the hydrogel. Silicon and PDMS are well studied on their biocompatiblity, especially for the application in microfluidic devices [77]. The use of the fluorophores Ruthenium(II)Dichloride and Nile blue chloride are also found biocompatible by various studies, like described earlier. The visualized 3D model that was fabricated by Kim et al., showed a cell viability of <90 % [59]. Implementing the model in a dynamic IoaC that has an improved *in vivo* like environment, may result in a higher cell viability.

The biocompatibility of the PHDs is expected to be high. PHDs are enzymes that are produced by the cells. The probes have proven a good cell viability in the study of Ning et al.

Sensor placement in the IoaC
The oxygen sensing microbeads are located in the microstructures of the intestinal cell scaffold. This allows spatial oxygen sensing over the total intestinal surface. However, the rate of dispersion of the microbeads over the ECM can deviate, due to the fabrication process of the hydrogel (insufficient mixing) or the printing nozzle. Calibration of the model will offer a solution to this. What could be a problem is the penetration depth of the used detection method. The choice to use NIR does increase the penetration depth, but it won't be sufficient enough to measure over the *in vivo* like structure of 1.6 mm. Therefore the intestinal tissue model needs to be miniaturized.

The PHDs are freely distributed over the surface of the chip. It does provide information about hypoxic vs. normoxic conditions, but no more.

Dimensions
Using extrusion bioprinting, structures in a range from 50-500 μm can be fabricated. This is needed, since the model needs to shrink in order to make it applicable for fluorescence assay. The maximum dimensions of the villi can be 800 μm. Although the Caco-2 cells can not be adjusted in diameter, the villi would still contain up to 8 cells in height.

The PHDs can flow in the constant fluidic flow of the IoaC, so the dimensions are equal to the chip used.

Response time
The microbeads have been used in the study of Wang et. al for real-time measurement of the oxygen level [78]. Using NIR, the response time can take up to 60 seconds. This time is longer than the required time of 10 seconds. The same applies to the use of the PHDs.

Endurance of regular deformations

About the endurance of regular deformations due to the applied mechanical stress on the hydrogel structure can only be speculated. Hydrogels are characterized as flexible structures [79]. PHDs are expected to endure the deformations. Probably the deformations let them be able to distribute themselfs easier over the surface.

Sensitivity The sensitivity of the microbeads in impeded by the shell and the integration in the hydrogel. Despite the high sensitivity of the Ruthenium(II)Dichloride for oxygen, the sensitivity of the construction would be not that high. The sensitivity of the probe in the Ning et al. study was high. However it can not be concluded if the same applies to this application.

	Mircobeads	**PHD probe**
Biocompatibility	Good	Good
Sensor Placement	Integrated in the tissue	Integrated in the tissue
Dimensions	Insufficient	Good
Response time	60 seconds	60 seconds
Endurance deformations	Good	Good
Sensitivity	Insufficient	Good

Table 2: This table provides an fast overview of the potential of the proposed solutions meeting the requirements set in Chapter 5

Additionally to the main requirements, there are some queries that are very important to mention. Regarding to the nice-to-have features, the sensor system wouldn't be able to calibrate itself, since the microbeads need to be fabricated every time again. Every time the fluorescence intensity of the microbeads can be different, resulting in a standard calibration of the chip before measuring. Looking at the integration of the sensor system, the system is easy integratable when using a bioprinter that can integrate several materials.

Finally, despite meeting the main requirements, there are a lot of additional disadvantages of the sensor system that need to be mentioned. Regarding to the detection method, fluorescence, it could be possible that background signals are generated by surrounding proteins, leading to an overestimation of the oxygen concentration [80]. NIR can overcome this disadvantage. The fabrication of the sensor system is very time-consuming and labor-intensive. It also requires a lot of equipment and is expected to be very expensive. The sensor can not be used for off-the-shelf production, which makes it not able to commercialize.

It is not known if the functionality of the PHDs is changed during the probe treatment, which can cause the enzym to dysfunction. Further investigation needs to be done.

8 Conclusion

The integration of optical sensing microbeads in a printable hydrogel has already been performed. However, the concept of printing a scaffold for the intestinal tissue in which these optical sensing microbeads were integrated, is to our knowledge a new application. Important for reliable results is an equally dispersion rate over in the scaffold. Connecting multiple detection sites over the radial axis of the intestinal layer and providing real-time information on the exact oxygen concentration,the oxygen gradient can be locally obtained. However, the technology is not found to be the ideal sensor for oxygen detection in IoaC application.

The PHDs are not found to fit the requirements of quantitatively measurement of the oxygen level, which makes them insufficient for the use a oxygen sensor in IoaC devices.

The most promising technique is the zero-consuption Clark electrode, providing a high selectivity for DO and it can be easily integrated within the IoaC.

References

[1] Barack H Obama. All Nobel Prizes, 2010.

[2] Pieter E. Oomen, Maciej D. Skolimowski, and Elisabeth Verpoorte. Implementing oxygen control in chip-based cell and tissue culture systems, 8 2016.

[3] Hyun Jung Kim, Dongeun Huh, Geraldine Hamilton, and Donald E. Ingber. Human gut-on-a-chip inhabited by microbial flora that experiences intestinal peristalsis-like motions and flow. *Lab on a Chip*, 12(12):2165–2174, 6 2012.

[4] Sasan Jalili-Firoozinezhad, Francesca S. Gazzaniga, Elizabeth L. Calamari, Diogo M. Camacho, Cicely W. Fadel, Amir Bein, Ben Swenor, Bret Nestor, Michael J. Cronce, Alessio Tovaglieri, Oren Levy, Katherine E. Gregory, David T. Breault, Joaquim M.S. Cabral, Dennis L. Kasper, Richard Novak, and Donald E. Ingber. A complex human gut microbiome cultured in an anaerobic intestine-on-a-chip. *Nature Biomedical Engineering*, 3(7):520–531, 7 2019.

[5] Jesus Shrestha, Sajad Razavi Bazaz, Hamidreza Aboulkheyr Es, Dania Yaghobian Azari, Benjamin Thierry, Majid Ebrahimi Warkiani, and Maliheh Ghadiri. Lung-on-a-chip: the future of respiratory disease models and pharmacological studies. *Critical Reviews in Biotechnology*, 40(2):213–230, 2 2020.

[6] Kai Wang, Kun Man, Jiafeng Liu, Yang Liu, Qi Chen, Yong Zhou, and Yong Yang. Microphysiological Systems: Design, Fabrication, and Applications, 6 2020.

[7] Qirui Wu, Jinfeng Liu, Xiaohong Wang, Lingyan Feng, Jinbo Wu, Xiaoli Zhu, Weijia Wen, and Xiuqing Gong. Organ-on-a-chip: Recent breakthroughs and future prospects, 2 2020.

[8] Nureddin Ashammakhi, Rohollah Nasiri, Natan Roberto de Barros, Peyton Tebon, Jai Thakor, Marcus Goudie, Amir Shamloo, Martin G. Martin, and Ali Khademhosseni. Gut-on-a-chip: Current progress and future opportunities, 10 2020.

[9] Sangeeta N. Bhatia and Donald E. Ingber. Microfluidic organs-on-chips, 8 2014.

[10] Pablo Giménez-Gómez, Rosalía Rodríguez-Rodríguez, Juan Manuel Ríos, Marta Pérez-Montero, Estrella González, Manuel Gutiérrez-Capitán, Jose Antonio Plaza, Xavier Muñoz-Berbel, and Cecilia Jiménez-Jorquera. A self-calibrating and multiplexed electrochemical lab-on-a-chip for cell culture analysis and high-resolution imaging. *Lab on a Chip*, 20(4):823–833, 2 2020.

[11] Gregory P. Donaldson, S. Melanie Lee, and Sarkis K. Mazmanian. Gut biogeography of the bacterial microbiota, 12 2015.

[12] Boyang Zhang, Anastasia Korolj, Benjamin Fook Lun Lai, and Milica Radisic. Advances in organ-on-a-chip engineering, 8 2018.

[13] Samad Ahadian, Robert Civitarese, Dawn Bannerman, Mohammad Hossein Mohammadi, Rick Lu, Erika Wang, Locke Davenport-Huyer, Ben Lai, Boyang Zhang, Yimu Zhao, Serena Mandla, Anastasia Korolj, and Milica Radisic. Organ-On-A-Chip Platforms: A Convergence of Advanced Materials, Cells, and Microscale Technologies, 1 2018.

[14] Yutaka Amao. Probes and Polymers for Optical Sensing of Oxygen, 2003.

[15] Katja N. Hoehn Elaine N. Marieb. Human Anatomy & Physiology, Global Edition - Elaine N. Marieb, Katja N. Hoehn. In *Human Anatomy & Physiology, Global Edition*, pages 909–911. 2015.

[16] Hans Clevers. XThe intestinal crypt, a prototype stem cell compartment, 7 2013.

[17] Tomohiro Kato and Robert L. Owen. Structure and function of intestinal mucosal epithelium. In *Mucosal Immunology, Two-Volume Set*, pages 131–151. Elsevier Inc., 2005.

[18] Karl S. Matlin and Michael J. Caplan. Epithelial Cell Structure and Polarity. In *Seldin and Giebisch's The Kidney*, pages 1–34. Elsevier Inc., 2008.

[19] Catherine A. Lozupone, Jesse I. Stombaugh, Jeffrey I. Gordon, Janet K. Jansson, and Rob Knight. Diversity, stability and resilience of the human gut microbiota, 9 2012.

[20] Susannah Selber-Hnativ, Belise Rukundo, Masoumeh Ahmadi, Hayfa Akoubi, and Et. Al. Human gut microbiota: Toward an ecology of disease, 7 2017.

[21] Phillipp Hartmann, Huikuan Chu, Yi Duan, and Bernd Schnabl. Gut microbiota in liver disease: Too much is harmful, nothing at all is not helpful either, 5 2019.

[22] Patrice Debré and Jean Yves Le Gall. Intestinal microbiota. *Bulletin de l'Academie Nationale de Medecine*, 198(9):1667–1684, 12 2014.

[23] Michael Graham Espey. Role of oxygen gradients in shaping redox relationships between the human intestine and its microbiota, 2 2013.

[24] Leon Zheng, Caleb J. Kelly, and Sean P. Colgan. Physiologic hypoxia and oxygen homeostasis in the healthy intestine. A review in the theme: Cellular responses to hypoxia. *American Journal of Physiology - Cell Physiology*, 309(6):C350–C360, 9 2015.

[25] Sandeep Sharma and Deepa Rawat. *Partial Pressure Of Oxygen (PO2)*. StatPearls Publishing, 9 2018.

[26] Pranjul Shah, Joëlle V. Fritz, Enrico Glaab, Mahesh S. Desai, Kacy Greenhalgh, Audrey Frachet, Magdalena Niegowska, Matthew Estes, Christian Jäger, Carole Seguin-Devaux, Frederic Zenhausern, and Paul Wilmes. A microfluidics-based in vitro model of the gastrointestinal human-microbe interface. *Nature Communications*, 7(1):11535, 5 2016.

[27] Amir Bein, Woojung Shin, Sasan Jalili-Firoozinezhad, Min Hee Park, Alexandra Sontheimer-Phelps, Alessio Tovaglieri, Angeliki Chalkiadaki, Hyun Jung Kim, and Donald E. Ingber. Microfluidic Organ-on-a-Chip Models of Human Intestine, 1 2018.

[28] Nureddin Ashammakhi, Rohollah Nasiri, Natan Roberto de Barros, Peyton Tebon, Jai Thakor, Marcus Goudie, Amir Shamloo, Martin G. Martin, and Ali Khademhosseni. Gut-on-a-chip: Current progress and future opportunities, 10 2020.

[29] Sebastiaan J. Trietsch, Elena Naumovska, Dorota Kurek, Meily C. Setyawati, Marianne K. Vormann, Karlijn J. Wilschut, Henriëtte L. Lanz, Arnaud Nicolas, Chee Ping Ng, Jos Joore, Stefan Kustermann, Adrian Roth, Thomas Hankemeier, Annie Moisan, and Paul Vulto. Membrane-free culture and real-time barrier integrity assessment of perfused intestinal epithelium tubes. *Nature Communications*, 8(1):1–8, 12 2017.

[30] Dongeun Huh, Hyun Jung Kim, Jacob P Fraser, Daniel E Shea, Mohammed Khan, Anthony Bahinski, Geraldine A Hamilton, and Donald E Ingber. Microfabrication of human organs-on-chips. *NATURE PROTOCOLS —*, 8(11), 2013.

[31] Usama Ismail. On the Fabrication and Development of Tissue on a Chip Devices On the Fabrication and Development of Tissue on a Chip Devices with Included Perfused Vasculatures with Included Perfused Vasculatures. Technical report, 2019.

[32] Dongeun Huh, Geraldine A. Hamilton, and Donald E. Ingber. From 3D cell culture to organs-on-chips, 12 2011.

[33] Douglas B. Weibel, Willow R. DiLuzio, and George M. Whitesides. Microfabrication meets microbiology, 3 2007.

[34] Qingzhen Yang, Qin Lian, and Feng Xu. Perspective: Fabrication of integrated organ-on-a-chip via bioprinting. *Biomicrofluidics*, 11(3), 5 2017.

[35] Marco PC Marques and Nicolas Szita. Bioprocess microfluidics: applying microfluidic devices for bioprocessing, 11 2017.

[36] Aslıhan Gökaltun, Young Bok (Abraham) Kang, Martin L. Yarmush, O. Berk Usta, and Ayse Asatekin. Simple Surface Modification of Poly(dimethylsiloxane) via Surface Segregating Smart Polymers for Biomicrofluidics. *Scientific Reports*, 9(1):1–14, 12 2019.

[37] Erika Ferrari, Cecilia Palma, Simone Vesentini, Paola Occhetta, and Marco Rasponi. Integrating Biosensors in Organs-on-Chip Devices: A Perspective on Current Strategies to Monitor Microphysiological Systems, 9 2020.

[38] Kyu Young Shim, Dongwook Lee, Jeonghun Han, Nam Trung Nguyen, Sungsu Park, and Jong Hwan Sung. Microfluidic gut-on-a-chip with three-dimensional villi structure. *Biomedical Microdevices*, 19(2):37, 6 2017.

[39] Tor Lea. Caco-2 cell line. In *The Impact of Food Bioactives on Health: In Vitro and Ex Vivo Models*, pages 103–111. Springer International Publishing, 1 2015.

[40] A. Moya, M. Ortega-Ribera, X. Guimerà, E. Sowade, M. Zea, X. Illa, E. Ramon, R. Villa, J. Gracia-Sancho, and G. Gabriel. Online oxygen monitoring using integrated inkjet-printed sensors in a liver-on-a-chip system. *Lab on a Chip*, 18(14):2023–2035, 7 2018.

[41] Roberta Poceviciute and Rustem F. Ismagilov. Human-gut-microbiome on a chip. *Nature Biomedical Engineering*, 3(7):500–501, 7 2019.

[42] Michael Eck. *Performance enhancement of hybrid nanocrystal-polymer bulk heterojunction solar cells : aspects of device efficiency, reproducibility, and stability.* PhD thesis, Albert-Ludwigs-Universität Freiburg, Breisgau, 1 2014.

[43] Samantha M. Grist, Lukas Chrostowski, and Karen C. Cheung. Optical oxygen sensors for applications in microfluidic cell culture, 10 2010.

[44] Woojung Shin, Alexander Wu, Miles W. Massidda, Charles Foster, Newin Thomas, Dong Woo Lee, Hong Koh, Youngwon Ju, Joohoon Kim, and Hyun Jung Kim. A robust longitudinal co-culture of obligate anaerobic gut microbiome with human intestinal epithelium in an anoxic-oxic interface-on-a-chip. *Frontiers in Bioengineering and Biotechnology*, 7(FEB), 2019.

[45] Ana Moya Lara Directores and Gemma Gabriel Buguña Eloi Ramon Garcia. Integrated sensors for overcoming Organ-On-a-Chip monitoring challenges Autor. Technical report, 2017.

[46] Elsbeth G B M Bossink, Olivier Y F Henry, Maximilian A Benz, Loes I Segerink, Donald E Ingber, Mathieu Odijk, Harvard John, and A Paulson. A MINIATURIZED CLARK OXYGEN SENSOR FOR ORGAN-ON-CHIP DEVICES. Technical report, 11 2018.

[47] Pieter E. Oomen, Maciej D. Skolimowski, and Elisabeth Verpoorte. Implementing oxygen control in chip-based cell and tissue culture systems, 2016.

[48] Ana Moya, Xavier Guimerà, Francisco Javier del Campo, Elisabet Prats-Alfonso, Antonio David Dorado, Mireia Baeza, Rosa Villa, David Gabriel, Xavier Gamisans, and Gemma Gabriel. Profiling of oxygen in biofilms using individually addressable disk microelectrodes on a microfabricated needle. *Microchimica Acta*, 182(5-6):985–993, 2015.

[49] Ching Chou Wu, Tomoyuki Yasukawa, Hitoshi Shiku, and Tomokazu Matsue. Fabrication of miniature Clark oxygen sensor integrated with microstructure. *Sensors and Actuators, B: Chemical*, 110(2):342–349, 10 2005.

[50] Ana Moya, Enrico Sowade, Francisco J. del Campo, Kalyan Y. Mitra, Eloi Ramon, Rosa Villa, Reinhard R. Baumann, and Gemma Gabriel. All-inkjet-printed dissolved oxygen sensors on flexible plastic substrates. *Organic Electronics*, 39:168–176, 12 2016.

[51] Fabian Liebisch, Andreas Weltin, Julia Marzioch, Gerald A. Urban, and Jochen Kieninger. Zero-consumption Clark-type microsensor for oxygen monitoring in cell culture and organ-on-chip systems. *Sensors and Actuators, B: Chemical*, 322:128652, 11 2020.

[52] J. Kieninger, F. Liebisch, A. Weltin, J. Marzioch, and G. A. Urban. Zero consumption clark-type oxygen microsensor for cell culture monitoring. In *TRANSDUCERS 2017 - 19th International Conference on Solid-State Sensors, Actuators and Microsystems*, pages 1497–1500. Institute of Electrical and Electronics Engineers Inc., 7 2017.

[53] Product: Oxygen Dipping Probe DP-PSt3.

[54] David I. Walsh, E. Victoria Dydek, Jaclyn Y. Lock, Taylor L. Carlson, Rebecca L. Carrier, David S. Kong, Catherine R. Cabrera, and Todd Thorsen. Emulation of Colonic Oxygen Gradients in a Microdevice. *SLAS Technology*, 23(2):164–171, 4 2018.

[55] Product: Profiling Oxygen Microsensor PM-PSt8.

[56] M. M. Stanton, J. Samitier, and S. Sánchez. Bioprinting of 3D hydrogels. *Lab on a Chip*, 15(15):3111–3115, 6 2015.

[57] Rasha H. Dosh, Nicola Jordan-Mahy, Christopher Sammon, and Christine L. Le Maitre. Long-term in vitro 3D hydrogel co-culture model of inflammatory bowel disease. *Scientific Reports*, 9(1), 12 2019.

[58] Justine Creff, Rémi Courson, Thomas Mangeat, J. Foncy, Sandrine Souleille, C. Thibault, Arnaud Besson, and Laurent Malaquin. Fabrication of 3D scaffolds reproducing intestinal epithelium topography by high-resolution 3D stereolithography. *Biomaterials*, 221:119404, 11 2019.

[59] Won Jin Kim and Geun Hyung Kim. An innovative cell-printed microscale collagen model for mimicking intestinal villus epithelium. *Chemical Engineering Journal*, 334:2308–2318, 2 2018.

[60] Lin Wang, Miguel A. Acosta, Jennie B. Leach, and Rebecca L. Carrier. Spatially monitoring oxygen level in 3D microfabricated cell culture systems using optical oxygen sensing beads. *Lab on a Chip*, 13(8):1586–1592, 2013.

[61] Richard Hayes, Adham Ahmed, Tony Edge, and Haifei Zhang. Core-shell particles: Preparation, fundamentals and applications in high performance liquid chromatography, 8 2014.

[62] Susan Y. Zhao and Benjamin S. Harrison. Morphology impact on oxygen sensing ability of Ru(dpp)3Cl2 containing biocompatible polymers. *Materials Science and Engineering C*, 53:280–285, 4 2015.

[63] Jeppe Madsen, Irene Canton, Nicholas J Warren, Efrosyni Themistou, Adam Blanazs, Burcin Ustbas, Xiaohe Tian, Russell Pearson, Giuseppe Battaglia, Andrew L Lewis, and Steven P Armes. Nile Blue-Based Nanosized pH Sensors for Simultaneous Far-Red and Near-Infrared Live Bioimaging. 2013.

[64] Gaurav Kaushik, Jeroen Leijten, and Ali Khademhosseini. Concise Review: Organ Engineering: Design, Technology, and Integration.

[65] Daniela Pranzo, Piero Larizza, Daniel Filippini, and Gianluca Percoco. Extrusion-based 3D printing of microfluidic devices for chemical and biomedical applications: A topical review, 7 2018.

[66] Amir K. Miri, Iman Mirzaee, Shabir Hassan, Shirin Mesbah Oskui, Daniel Nieto, Ali Khademhosseini, and Yu Shrike Zhang. Effective bioprinting resolution in tissue model fabrication. *Lab on a Chip*, 19(11):2019–2037, 6 2019.

[67] Victor Hernandez-Gordillo, Abigail N. Koppes, Linda G. Griffith, David T. Breault, and Rebecca L. Carrier. Engineering the Niche for Intestinal Regeneration. In *Biology and Engineering of Stem Cell Niches*, pages 601–615. Elsevier Inc., 4 2017.

[68] Ammar Abdo and Mesut Sahin. NIR light penetration depth in the rat peripheral nerve and brain cortex. In *Annual International Conference of the IEEE Engineering in Medicine and Biology - Proceedings*, volume 2007, pages 1723–1725. NIH Public Access, 2007.

[69] Amato J. Giaccia, M. Celeste Simon, and Randall Johnson. The biology of hypoxia: The role of oxygen sensing in development, normal function, and disease. In *Genes and Development*, volume 18, pages 2183–2194. Cold Spring Harbor Laboratory Press, 9 2004.

[70] Patrick Pollard, Ming Yang, Huizhong Su, Tomoyoshi Soga, and Kamil Kranc. Prolyl hydroxylase domain enzymes: important regulators of cancer metabolism. *Hypoxia*, 2:127, 8 2014.

[71] Eric Metzen, Utta Berchner-Pfannschmidt, Petra Stengel, Jan H. Marxsen, Ineke Stolze, Matthias Klinger, Wei Qi Huang, Christoph Wotzlaw, Thomas Hellwig-Bürgel, Wolfgang Jelkmann, Helmut Acker, and Joachim Fandrey. Intracellular localisation of human HIF-1α hydroxylases: Implications for oxygen sensing, 4 2003.

[72] Edurne Berra, Emmanuel Benizri, Amandine Ginouvès, Véronique Volmat, Danièle Roux, and Jacques Pouysségur. HIF prolyl-hydroxylase 2 is the key oxygen sensor setting low steady-state levels of HIF-1α in normoxia. *EMBO Journal*, 22(16):4082–4090, 8 2003.

[73] Toru Komatsu, Kazuya Kikuchi, Hideo Takakusa, Kenjiro Hanaoka, Tasuku Ueno, Mako Kamiya, Yasuteru Urano, and Tetsuo Nagano. Design and synthesis of an enzyme activity-based labeling molecule with fluorescence spectral change. *Journal of the American Chemical Society*, 128(50):15946–15947, 12 2006.

[74] Jing Ning, Wei Wang, Guangbo Ge, Peng Chu, Feida Long, Yongliang Yang, Yulin Peng, Lei Feng, Xiaochi Ma, and Tony D. James. Target Enzyme-Activated Two-Photon Fluorescent Probes: A Case Study of CYP3A4 Using a Two-Dimensional Design Strategy. *Angewandte Chemie - International Edition*, 58(29):9959–9963, 7 2019.

[75] Fritjof Helmchen and Winfried Denk. Deep tissue two-photon microscopy, 12 2005.

[76] Julius Z.H. von Martels, Mehdi Sadaghian Sadabad, Arno R. Bourgonje, Tjasso Blokzijl, Gerard Dijkstra, Klaas Nico Faber, and Hermie J.M. Harmsen. The role of gut microbiota in health and disease: In vitro modeling of host-microbe interactions at the aerobe-anaerobe interphase of the human gut, 4 2017.

[77] Sophie L. Peterson, Anthony McDonald, Paul L. Gourley, and Darryl Y. Sasaki. Poly(dimethylsiloxane) thin films as biocompatible coatings for microfluidic devices: Cell culture and flow studies with glial cells. *Journal of Biomedical Materials Research - Part A*, 72(1):10–18, 1 2005.

[78] Lin Wang, Miguel A. Acosta, Jennie B. Leach, and Rebecca L. Carrier. Spatially monitoring oxygen level in 3D microfabricated cell culture systems using optical oxygen sensing beads. *Lab on a Chip*, 13(8):1586–1592, 3 2013.

[79] Hikmet Geckil, Feng Xu, Xiaohui Zhang, Sangjun Moon, and Utkan Demirci. Engineering hydrogels as extracellular matrix mimics, 4 2010.

[80] Christopher P. Toseland. Fluorescent labeling and modification of proteins, 7 2013.

[81] Miguel A. Acosta, Patrick Ymele-Leki, Yordan V. Kostov, and Jennie B. Leach. Fluorescent microparticles for sensing cell microenvironment oxygen levels within 3D scaffolds. *Biomaterials*, 30(17):3068–3074, 6 2009.

9 Appendix

9.1 Protocol microbead integrated hydrogel production

This protocol includes the total fabricating process for the production of a microbead integrated hydrogel. This protocol is based on the fabricating processes described in [81].

9.1.1 Fabrication of the microbeads

Day 1

1. Stir a suspension of 2 g of silica gel (Davisil 710, 9.5–11 µm-diameter) and 40 mL of 0.01 N NaOH for 30 min.
2. Add simultaneously 10 mL of a 0.5 mm solution (in ethanol) of the oxygen-sensitive ruthenium (II) dichloride and 10 mL of a 0.5 mm solution (also in ethanol) of the oxygen-insensitive Nile blue chloride.
3. Stir the mixture for another 30 min.
4. Centrifuge the solution for 20 min at 1900g to remove the supernatant.
5. Wash the remaining particles and centrifuged three times in 30 mL of deionized water and once in 30 mL of ethanol. After removal of the supernatant, dry the particles at 70 °C overnight.

Day 2

1. Vortex a solution of 0.2 g of the dry luminophore-bound silica gel particles, 700 µL of hexane, 1 g of PDMS pre-polymer, and 0.1 g of curing agent for 1 min.
2. Heat a 2 w/v% solution of sodium dodecyl sulfate (SDS) in water (300 mL) in a hot-plate to 70 °C and magnetically stir the solution at 1200 rpm using a 3.81cm stir bar.
3. Pour the silica gel/PDMS solution into the SDS solution and heat and stir the resulting oil-in-water emulsion for 7–8 h.
4. Strain the emulsion twice; first through a 0.5-mm sieve and then through a 25-µm sieve.
5. Wash the particles collected by the 25-µm sieve and centrifuge three times in 30 mL of a 0.2 w/v % bovine serum albumin (BSA) in phosphate-buffered saline (PBS) solution with 0.1% methyl-4-hydroxybenzoate for 20 min at 1900 g.
6. After the final washing step, re-suspend the particles to a density of 50 particles/µL in 0.2% BSA in PBS and store in the dark at 4 °C.

9.1.2 Fabrication of the microbead integrated hydrogel

Day 1

Dry 10 g of PEG of adsorbed water using azeotropic distillation in toluene (4 mL/g PEG), concentrated, and then dried overnight under vacuum.

Day 2

1. Add dry pyridine (3 mL/g PEG) under an argon purge to dissolve the PEG.
2. Cool the solution to 0 °C in an ice bath.
3. Add methacrylic anhydride (4 molar excess to the moles of PEG) slowly with a syringe to the PEG/pyridine solution still in the ice bath.
4. Mix the new solution in an ice bath for 10 min and then allow to react for 48 h in the dark at room temperature.

Day 3

1. Work in minimal light and dilute the reaction 10–15× with dichloromethane and wash twice with 1 m HCl to neutralize the reaction byproducts.
2. Dry the dichloromethane/PEG-DM solution was dried with sodium sulfate, filter and concentrate to 50 mL, precipitate in ice-cold diethyl ether, filter, and dry overnight under vacuum in the dark at room temperature. Store the PEG-DM product with desiccant at 20 °C.